

# Vision-LLMs for Spatiotemporal Traffic Forecasting

Ning Yang, Hengyu Zhong, Haijun Zhang, Randall Berry

**Abstract**—Accurate spatiotemporal traffic forecasting is a critical prerequisite for proactive resource management in dense urban mobile networks. While Large Language Models (LLMs) have shown promise in time series analysis, they inherently struggle to model the complex spatial dependencies of grid-based traffic data. Effectively extending LLMs to this domain is challenging, as representing the vast amount of information from dense geographical grids can be inefficient and overwhelm the model’s context. To address these challenges, we propose **ST-Vision-LLM**, a novel framework that reframes spatiotemporal forecasting as a vision-language fusion problem. Our approach leverages a Vision-LLM visual encoder to process historical global traffic matrices as image sequences, providing the model with a comprehensive global view to inform cell-level predictions. To overcome the inefficiency of LLMs in handling numerical data, we introduce an efficient encoding scheme that represents floating-point values as single tokens via a specialized vocabulary, coupled with a two-stage numerical alignment fine-tuning process. The model is first trained with Supervised Fine-Tuning (SFT) and then further optimized for predictive accuracy using Group Relative Policy Optimization (GRPO), a memory-efficient reinforcement learning method. Evaluations on real-world mobile traffic datasets demonstrate that ST-Vision-LLM outperforms existing methods by 15.6% in long-term prediction accuracy and exceeds the second-best baseline by over 30.04% in cross-domain few-shot scenarios. Our extensive experiments validate the model’s strong generalization capabilities across various data-scarce environments.

**Index Terms**—Spatiotemporal traffic forecasting, Large Language Models (LLMs), Vision-language fusion, Reinforcement learning, Few-shot learning, Mobile networks.

## I. INTRODUCTION

**T**HE ever-increasing demand for high-speed, reliable mobile connectivity in dense urban environments presents a significant challenge for network operators. Meeting this demand hinges on proactive resource management, for which accurate traffic prediction is a critical prerequisite [1]. The evolution of spatiotemporal sequence prediction has progressed from classical statistical methods to more advanced deep learning approaches. Early deep learning efforts utilized sequence models, such as those based on recurrent or temporal convolutional architectures, which demonstrated proficiency in capturing temporal patterns for tasks like traffic flow prediction

[2], [3]. To better address data with explicit spatial structures, subsequent research integrated graph-based techniques. These graph neural network models leverage mechanisms like graph convolutions and attention to simultaneously model complex spatial and temporal dependencies [4], [5]. Although these methods have achieved promising results in their respective application scenarios, they often require meticulous architectural design tailored to specific datasets and tasks, thus exhibiting limited generalization capabilities across different scenarios [6], [7].

Inspired by the success of large-scale pre-trained models in computer vision (CV) and natural language processing (NLP), researchers have begun exploring general-purpose time series analysis models. Foundation models, particularly those based on the transformer architecture, have shown superb performance by leveraging self-attention mechanisms and sophisticated input representations to enhance long-term prediction capabilities [7], [8]. Similarly, methods that adapt Large Language Models (LLMs) for time series forecasting have emerged, harnessing the powerful representation and reasoning abilities of LLMs through techniques like text-based prompting or fine-tuning [9], [10]. However, despite their proficiency in capturing intricate temporal dependencies and patterns, these general-purpose approaches often fall short in modeling the complex spatial associations and topological structures inherent in spatiotemporal traffic data [10], [11].

Recognizing this limitation, several recent works have attempted to bridge the gap by integrating spatial structural information with LLMs. These approaches generally involve strategies such as augmenting the input sequence with specialized spatiotemporal positional encodings [12], tokenizing graph-structured neighborhoods for processing by the LLM [13], and directly modifying the core attention mechanism or adding adapter modules to inject a spatial bias [14]. A parallel line of work uses dedicated spatiotemporal encoders to pre-process the data before instruction-tuning the LLM [15]. However, these methods face a common set of challenges. They either append spatial information as linear sequences, which can be an inefficient representation that struggles with information compression, or they necessitate substantial modifications to the model’s core architecture to handle spatiotemporal features [12]–[15]. Such intrusive approaches risk constraining the model’s ability to leverage the full reasoning and generalization capabilities inherent in the pre-trained LLM.

The central challenge is thus to integrate complex spatial dependencies into an LLM framework without resorting to inefficient data representations or compromising the integrity of the pre-trained model’s architecture. To overcome this, we propose the **Spatiotemporal Vision Large Language Model (ST-Vision-LLM)** framework, which reframes the spatiotemporal sequence prediction task as a vision-language fusion

Ning Yang is with the Institute of Automation, Chinese Academy of Sciences, Beijing, 100190, China (e-mail: ning.yang@ia.ac.cn).

Hengyu Zhong is with Westa College, Southwest University, Chongqing, 400715, China. This work was performed while he was an intern at the Institute of Automation, Chinese Academy of Sciences (e-mail: hengyuzhong@126.com).

Haijun Zhang is with the Department of Computing and Communication Engineering, Beijing University of Science and Technology, Beijing, 100083, China (e-mail: zhanghaijun@ustb.edu.cn).

Randall Berry is with the Department of Electrical and Computer Engineering, Northwestern University, Chicago, 60208, USA (e-mail: rberry@northwestern.edu).

(Corresponding author: Ning Yang.)

problem. Instead of treating spatial locations as a discrete list, ST-Vision-LLM employs a visual encoder to transform historical global traffic matrix sequences into holistic image-like representations. These visual embeddings are then integrated into the context of a Vision-LLM, enabling the model to perceive and reason about comprehensive global spatiotemporal patterns as a unified scene, thereby naturally capturing spatial relationships during cell-level predictions. To address the inefficient representation of numerical values in standard LLMs, we design a float-specific vocabulary that encodes numbers into single tokens, significantly conserving context length. We then perform a two-stage numerical alignment fine-tuning process to enable the model to comprehend and generate these new numerical tokens. With this enhanced numerical capability established, we first conduct supervised fine-tuning on spatiotemporal traffic data, followed by policy optimization using a memory-efficient reinforcement learning algorithm [16], to further refine and improve prediction accuracy.

**Our main contributions include:**

- 1) We propose the ST-Vision-LLM, a novel framework that reframes spatially correlated spatiotemporal sequence prediction as a vision-language fusion task. This approach transforms the prediction problem into a sequence generation task within a multimodal context.
- 2) Our work introduces the ST-Vision-LLM architecture, which embeds global historical spatiotemporal information into the LLM context via a visual encoder. This framework also introduces an efficient numerical token encoding and an aligned fine-tuning strategy, enabling the model to perform cell-level traffic prediction based on a complete global view.
- 3) The effectiveness of our approach is validated on multiple real-world mobile network spatiotemporal datasets. The results demonstrate that ST-Vision-LLM surpasses existing methods in long-term prediction accuracy and exhibits outstanding performance in few-shot and zero-shot scenarios, offering an effective solution for spatiotemporal traffic prediction in data-scarce environments.

## II. RELATEDWORK

### A. Task-Specific Learning

Traditional spatiotemporal sequence prediction methods are often customized for specific tasks and domains, training models end-to-end on small-scale datasets. Early efforts in spatiotemporal sequence prediction began by adapting models from time series analysis. For example, the classical statistical model Autoregressive Integrated Moving Average (ARIMA) was applied to traffic flow prediction [18], but its linearity struggled with complex dynamics. To address this, deep learning models were introduced. Recurrent networks like Long Short-Term Memory (LSTM) could capture non-linear temporal dependencies, with hybrid models like ResLSTM [19] combining it with residual and graph convolutional networks. Convolutional networks such as Temporal Convolutional Networks (TCNs) proved effective for long sequences, and architectures like ST-ResNet [20] utilized residual networks to

model various temporal properties. However, these models primarily focused on temporal patterns, neglecting spatial correlations.

To address this spatial oversight, researchers began integrating graph neural networks. Initial works like Diffusion Convolutional Recurrent Neural Network (DCRNN) and Spatio-Temporal Graph Convolutional Networks (STGCN) [21] combined graph convolutions with recurrent or convolutional layers to simultaneously model predefined spatial and temporal dependencies. Yet, their reliance on a static, predefined graph structure limited their ability to capture dynamic spatial correlations, leading subsequent research to introduce adaptive adjacency matrices that enable models like Graph WaveNet (GWN) [22] to learn spatial dependencies directly from data. Further variations like Multi-Component Spatio-Temporal Graph Convolution Networks (MSTGCN) [23] were developed to capture correlations across different time periods. Concurrently, attention mechanisms were incorporated to weigh the importance of different spatiotemporal relationships, as seen in the Graph Multi-Attention Network (GMAN). Another example is Attentive Crowd Flow Machine (ACFM) [24], which uses an attention mechanism composed of two progressive ConvLSTM units. Despite these advancements in capturing intricate spatiotemporal patterns, these methods are typically designed and trained end-to-end for narrow, specific tasks (e.g., Spatio-Temporal Network (STN) for mobile traffic [6]), which often results in poor generalization to diverse time series data.

### B. Time Series Level General Learning

Inspired by the success of the pre-training and fine-tuning paradigm in CV and NLP, recent years have seen exploration into general models at the time series level. Some works attempt to pre-train universal representations on large-scale time series data, then transfer to downstream tasks. Early efforts focused on enhancing the Transformer architecture for long-term forecasting, with models like Informer, Autoformer, and FEDformer designed to improve efficiency and handle long dependencies. A significant conceptual shift came with Patch Time Series Transformer (PatchTST), which tokenizes time series into sub-sequence “patches”, allowing Transformers to better capture local semantic information.

This breakthrough paved the way for leveraging the power of pre-trained LLMs. Frozen Pretrained Transformer (FPT) demonstrated that even a frozen pre-trained Transformer can achieve strong performance by only fine-tuning the head and tail. Further works like Time-LLM [10] and LLM4TS explored reprogramming and fine-tuning strategies to align LLMs with time series data, unlocking powerful few-shot and zero-shot capabilities. While models like iTransformer further refined the architecture to better capture multivariate correlations, these generalist approaches are fundamentally designed for one-dimensional (1D) sequences. They inherently lack the mechanisms to model the complex topological structures and spatial correlations present in two-dimensional (2D) grid-based spatiotemporal data. Related work also includes pre-training time series foundation models from scratch, such as TimesFM

(2024), CHRONOS, and MOMENT, which train models using large-scale time series data and achieve significant prediction performance in zero-shot and few-shot scenarios. In summary, these methods primarily focus on capturing temporal dependencies and patterns in time series data but generally lack spatial modeling capabilities, making them unsuitable for scenarios requiring complex spatial analysis.

### C. Spatiotemporal Series Level General Learning

Recognizing the importance of spatial correlations, recent works have combined spatial information with LLMs for spatiotemporal sequence prediction. These approaches generally follow two main strategies. One strategy involves using separate, specialized encoders to process spatial and temporal features before feeding them to an LLM. UrbanGPT, for instance, uses a temporal convolutional encoder, while Traffic Prediction LLM (TPLLM) employs both convolutional and graph convolutional networks. A second, more integrated strategy aims to make the LLM itself spatially aware. This is often achieved by either enriching the input with positional information, as seen in Spatial-Temporal Large Language Model (ST-LLM) [12], or by designing novel tokenizers like the graph-based tokenizer in STG-LLM. Other approaches fuse graph neural networks with LLMs, such as GCNGPT [12], which combines GCN with a pre-trained Transformer, and GATGPT [25], which integrates graph attention mechanisms. Some approaches, including ST-LINK, even modify the core attention mechanism to explicitly encode spatial relationships.

However, these methods are primarily designed for data with discrete, node-based spatial structures, such as traffic sensor networks. Their effectiveness is constrained when applied to large-scale, grid-based data, where the perceptual region is vast and dense. The sheer number of grid cells makes node-centric graph representations or direct positional encodings computationally prohibitive and inefficient, limiting their ability to perceive and model patterns over a large spatial area. Unlike existing methods, we neither limit ourselves to merely adding position encoding to traffic data without compression, nor do we need to significantly modify model structures to design specialized encoders for traffic data compression. Instead, we leverage visual encoders to transform 2D spatiotemporal sequence information based on geographic grids into contextual inputs for Vision-LLMs, a strategy designed to fully unleash their inherent reasoning and generalization capabilities.

## III. 2D SPATIOTEMPORAL TRAFFIC FORECASTING PROBLEM

To formally define the 2D spatiotemporal traffic forecasting problem, we model the urban area as a regular geographical grid of size  $H \times W$ , where  $H$  and  $W$  are the height and width of the grid, respectively. The mobile network usage across this grid at a given time step is captured as a traffic matrix. The core task is to forecast the traffic matrices for the next  $K$  future time steps, given a history of observed traffic matrices over the past  $S$  time steps. We denote the complete sequence of traffic data observed over a time interval of length  $T$  as

$\mathbf{D} = \{D_1, D_2, \dots, D_T\}$ , where  $D_t$  represents a snapshot of mobile traffic at time  $t$  over the  $H \times W$  geographical grid, specifically expressed as:

$$D_t = \begin{bmatrix} d_t^{(1,1)} & \dots & d_t^{(1,W)} \\ \vdots & \ddots & \vdots \\ d_t^{(H,1)} & \dots & d_t^{(H,W)} \end{bmatrix}, \quad (1)$$

where  $d_t^{(x,y)}$  denotes the network usage metric value at geographical grid coordinates  $(x, y)$ , such as internet bandwidth, call frequency, or short message service (SMS) transmission rates. The spatiotemporal traffic prediction task involves forecasting mobile communication traffic across all geographical grids for the next  $K$  time steps, given  $S$  observed values of  $D_t$ . This can be formulated as:

$$\tilde{\mathbf{D}}_{t+1:t+K} = \arg \max_{\mathbf{D}_{t+1:t+K}} p(\mathbf{D}_{t+1:t+K} | \mathbf{D}_{t-S+1:t}), \quad (2)$$

where  $\mathbf{D}_{t+1:t+K} = \{\mathbf{D}_{t+1}, \mathbf{D}_{t+2}, \dots, \mathbf{D}_{t+K}\}$  represents the sequence of future traffic matrices across all grid cells, spanning the time interval from  $t+1$  to  $t+K$ , i.e., the forecast target for the next  $K$  time steps. Given the inherent output-length constraints of current LLMs, our approach encodes the full spatiotemporal history  $\mathbf{D}_{t-S+1:t} = \{\mathbf{D}_{t-S+1}, \dots, \mathbf{D}_t\}$  while generating forecasts on a per-cell basis. This per-cell generation strategy is underpinned by a simplifying assumption, inspired by the conditional factorization in Conditional Neural Processes [26], that the future states of individual grid cells are conditionally independent when conditioned on the global history  $\mathbf{D}_{t-S+1:t}$ . Under this assumption, the future of each cell is primarily determined by the global history  $\mathbf{D}_{t-S+1:t}$  and its own coordinates  $(x, y)$ . Adopting this approximation allows the problem to be framed as the following decomposition:

$$p(\mathbf{D}_{t+1:t+K} | \mathbf{D}_{t-S+1:t}) \approx \prod_{x=1}^H \prod_{y=1}^W p(\mathbf{d}_{t+1:t+K}^{(x,y)} | \mathbf{D}_{t-S+1:t}, (x, y)), \quad (3)$$

Consequently, the original task can be decomposed into multiple cell-level prediction subtasks. For any coordinates  $(x, y)$  in the geographical grid, where  $x \in \{1, 2, \dots, H\}$  and  $y \in \{1, 2, \dots, W\}$ , the cell-level prediction solved by the LLM can be formulated as:

$$\tilde{\mathbf{d}}_{t+1:t+K}^{(x,y)} = \arg \max_{\mathbf{d}_{t+1:t+K}^{(x,y)}} p(\mathbf{d}_{t+1:t+K}^{(x,y)} | \mathbf{D}_{t-S+1:t}, (x, y)), \quad (4)$$

Here,  $\mathbf{d}_{t+1:t+K}^{(x,y)} = \{d_{t+1}^{(x,y)}, d_{t+2}^{(x,y)}, \dots, d_{t+K}^{(x,y)}\}$  represents the sequence of future traffic values for the single cell at coordinates  $(x, y)$  over the next  $K$  time steps. By performing predictions across all  $H \times W$  geographical grids, we can reconstruct the complete spatiotemporal traffic sequence:

$$\tilde{D}_{t+k} = \begin{bmatrix} \tilde{d}_{t+k}^{(1,1)} & \dots & \tilde{d}_{t+k}^{(1,W)} \\ \vdots & \ddots & \vdots \\ \tilde{d}_{t+k}^{(H,1)} & \dots & \tilde{d}_{t+k}^{(H,W)} \end{bmatrix}, \quad k = 1, 2, \dots, K, \quad (5)$$

where  $\tilde{D}_{t+k}$  represents the predicted value of  $D_{t+k}$ .

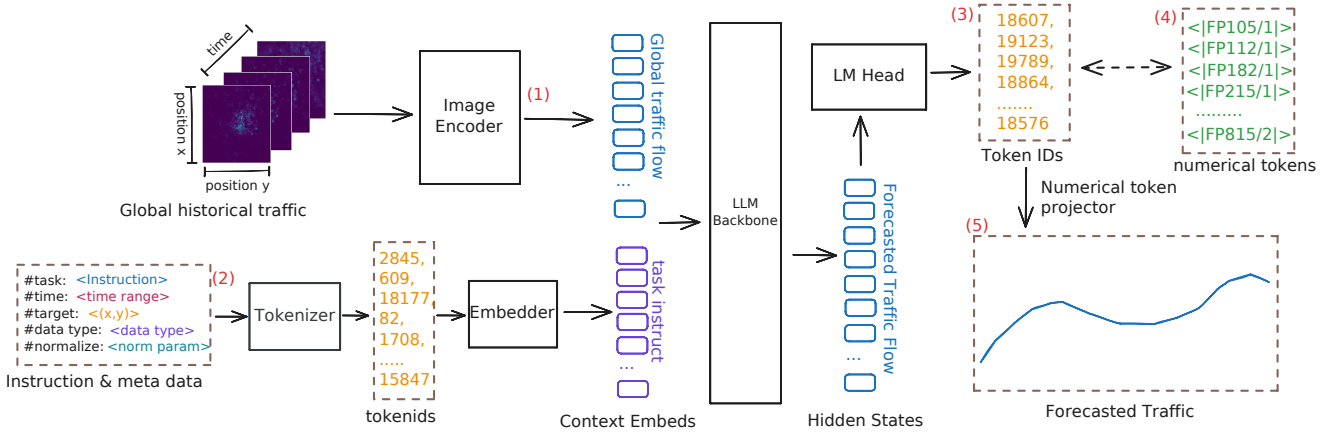


Fig. 1. **The ST-Vision-LLM Framework.** Given global historical spatiotemporal traffic information, we first normalize the spatiotemporal traffic data, then input it into (1) the image encoder of the multimodal LLM to obtain encoded information in the form of image patches, which are subsequently fed into the LLM’s context embedding. Simultaneously, we input (2) the target geographic grid, metadata, and task instructions in textual form, which are processed through a text tokenizer and embedding before being fed into the LLM context. Subsequently, the LLM performs inference and outputs predicted future traffic information in the form of (3) numerical tokens (where (3) represents the token IDs output by the LLM, and (4) represents the human-readable labels of the numerical tokens corresponding to the token IDs). Finally, the (3) numerical tokens are mapped to (5) the final traffic forecasting results through a numerical token mapper, which represents the future traffic sequence predictions for the current geographic grid.

## IV. METHODOLOGY

### A. The ST-Vision-LLM Framework

The ST-Vision-LLM framework formulates city-wide 2D spatiotemporal traffic prediction as a vision-language task. The proposed method predicts future  $K$ -step traffic at the cell level, conditioned on a sequence of  $S$  historical frames of global traffic information  $\mathbf{D}_{t-S+1:t}$ . Formally, the objective for each target cell with geographic coordinates  $(x, y)$  is to solve the optimization problem defined in Equation (4).

The proposed methodology is composed of three core components. First, the input processing module constructs a multimodal context. The historical spatiotemporal traffic sequence  $\mathbf{D}_{t-S+1:t}$  is processed by the image encoder of a foundation Vision-LLM. This process yields a sequence of visual embeddings, which serve as visual input to the context of the LLM. Concurrently, the associated metadata for the target cell  $(x, y)$  and its historical scalar sequence are formatted into a textual prompt. This prompt is then tokenized and provided as textual input to the same context.

Second, to overcome the inherent inefficiency of LLMs in processing continuous numerical data, we introduce an efficient numerical encoding scheme. This scheme features a specialized floating-point vocabulary and an alignment fine-tuning strategy, enabling the representation of numerical values as single tokens. This allows the LLM to directly output the predicted traffic sequence  $\tilde{\mathbf{d}}_{t+1:t+K}^{(x,y)}$  as specialized numerical tokens, thereby conserving context length and improving computational efficiency.

Finally, we employ a two-stage training process for the optimization of predictive performance. The model first undergoes SFT to learn the fundamental spatiotemporal dynamics from the traffic data. Subsequently, the model is further refined via policy optimization, specifically using GRPO, to enhance its predictive capabilities and final performance.

### B. Direct Numerical Encoding Method

1) *Numerical Token Design:* A significant challenge in applying LLMs to numerical tasks is their inherent inefficiency in processing floating-point numbers, which are typically tokenized into multiple, less meaningful character-level tokens. To overcome this limitation and enhance both training and inference efficiency by compressing sequence length, we propose a direct numerical encoding method for the efficient encoding of floating-point numbers into single tokens, thereby representing real numbers in a discrete vocabulary space. This method is inspired by Charton (2022) [27], and its primary advantage lies in its ability to represent floating-point numbers of varying precision as a single token, thus significantly compressing the sequence length of numerical data in the model’s input.

In particular, we construct a dedicated numerical vocabulary,  $V_{FP}$ , composed of a series of special numerical tokens of the form  $\langle \text{FP } m/b \rangle$ . Here, “FP” is an abbreviation for “Floating-Point,” serving to identify the string as a special token that represents a floating-point value. In this format,  $m$  represents the integer mantissa, and  $b$  represents the base-10 exponent. The mapping from these numerical tokens to their corresponding floating-point values is defined as:

$$\langle \text{FP } m/b \rangle \mapsto \text{Norm}(m) \times 10^b, \quad (6)$$

Here,  $\text{Norm}(m)$  is a normalization function that converts the integer  $m$  into its scientific notation form by placing the decimal point after the first significant digit. This function decouples the magnitude of the final floating-point number from the magnitude of  $m$ , ensuring that the magnitude of the final floating-point number is determined solely by the exponent  $b$ . This operation is formally defined as:

$$\text{Norm}(m) = \frac{m}{10^{\lfloor \log_{10} |m| \rfloor}}, \quad (7)$$

We set the range for  $m$  to  $\{-9999, \dots, -10\} \cup \{10, \dots, 9999\}$  and the range for the exponent  $b$  to  $\{-4, \dots, 5\}$ , a selection

designed to cover the numerical dynamic range common in our task and based on the numerical distribution of traffic data in the Telecom Italia Big Data Challenge [38] dataset, where the term  $10^{\lfloor \log_{10} |m| \rfloor}$  serves as a normalization divisor to place the decimal point after the first significant digit of  $m$ . By iterating through all possible  $(m, b)$  combinations, we construct a numerical vocabulary that covers a wide dynamic range.

We define a single token representing a floating-point number encoded via this method as a **numerical token**. Compared to representing numbers as direct string sequences, this single-token encoding method significantly reduces sequence length, thereby enhancing the model’s training and inference efficiency.

2) *Numerical Alignment Fine-tuning Method*: Having designed a specialized vocabulary for numerical values, the next critical step is to imbue the pre-trained LLM with the ability to comprehend and generate these new tokens. Unlike Charton (2022) [27], who trained LLMs from scratch using pure numerical tokens for linear algebra tasks, our research focuses on fine-tuning pre-trained LLMs to understand and generate numerical tokens. A numerical alignment fine-tuning method is proposed to realize this goal, enabling conventional pre-trained LLMs to acquire the capability of processing numerical tokens and executing downstream tasks.

The numerical fine-tuning method comprises two stages: semantic alignment fine-tuning and basic arithmetic alignment fine-tuning. In the first stage, we embed the numerical vocabulary  $V_{FP}$  into the input and output embedding layers of the LLMs and fine-tune the embedding layers to achieve semantic alignment between numerical tokens and text-represented floating-point numbers in semantic space. In the second stage, we construct simple linear algebra operation datasets using a mixture of numerical tokens and text-represented floating-point numbers, and perform SFT on this dataset to enable the LLM to execute basic operations using numerical tokens.

### Stage 1: Semantic Alignment Fine-tuning

Having established the vocabulary, the immediate challenge is to train the newly initialized parameters within the word embedding layer, enabling the model to comprehend these new tokens. The primary goal of this stage is to bridge the semantic gap between our newly introduced numerical tokens and the model’s pre-existing understanding of numbers represented as text. To achieve this, we first extend the LLM’s input and output embedding matrices to include  $V_{FP}$ . Then align the newly initialized numeric embeddings with their textual numerical counterparts so that, for instance,  $\langle |FP114/0| \rangle$  and the string “1.14” occupy nearby positions in the semantic space. This process ensures that the model interprets the new numerical token not as an arbitrary symbol, but as a meaningful representation of a quantity, semantically grounding it within the model’s existing understanding of numbers. To this end, we freeze the backbone and fine-tune only the input/output embeddings on transcription tasks, establishing a bidirectional mapping between textual numerals and numeric tokens. Example prompts:

- “Convert the following string-represented numerical value to numerical tokens: ‘-82.100000’  $\rightarrow$   $\langle |FP-821/1| \rangle$ ”

- “Transcribe the following numerical token to string numerical value:  $\langle |FP114/2| \rangle \rightarrow$  ‘114.000000’ ”

Through training in this stage, numerical tokens achieve basic alignment with text-represented floating-point numbers in semantic space, acquiring reasonable numerical representation capabilities.

### Stage 2: Basic Arithmetic Alignment Fine-tuning

While the semantic alignment in Stage 1 endows the numerical tokens with meaning, it does not equip the model with the ability to perform more complex mathematical tasks using these tokens. To bridge this gap and equip the model with the quantitative reasoning abilities essential for traffic forecasting, we proceed to the second stage. The objective of this phase is to equip the LLM with the ability to perform basic arithmetic operations, thereby enhancing its performance in handling numerical tokens for the traffic forecasting task. To this end, we train the model through continuous fine-tuning on numerical computation tasks. This process involves unfreezing and adjusting the model’s backbone, token embedding layer, and output layer to obtain more precise vector representations. Considering that the model backbone is pre-trained and the newly initialized embedding and output layers have undergone preliminary alignment, we apply the Low-Rank Adaptation (LoRA) [28] method for parameter-efficient fine-tuning of the backbone, embedding, and output layers.

This fine-tuning is applied to a preexisting LLM. Given that pre-trained models already possess foundational mathematical abilities [29], our training does not involve complex mathematical tasks, but rather concentrates on three fundamental linear algebra operations that can effectively inject numerical capabilities through a few templated examples [30] while respectively covering key mechanisms in the Transformer architecture, such as approximate linear estimation [31] and native element-wise interactions [32]: vector addition, vector subtraction, and the Hadamard product. For vectors  $\mathbf{a} = [a_1, \dots, a_n]$  and  $\mathbf{b} = [b_1, \dots, b_n]$ :

- Addition:  $\mathbf{a} + \mathbf{b} = [a_1 + b_1, \dots, a_n + b_n]$ .
- Subtraction:  $\mathbf{a} - \mathbf{b} = [a_1 - b_1, \dots, a_n - b_n]$ .
- Hadamard Product:  $\mathbf{a} \odot \mathbf{b} = [a_1 b_1, \dots, a_n b_n]$ .

Each task includes a combination of three input-output formats: numerical tokens to numerical strings, numerical strings to numerical tokens, and numerical tokens to numerical tokens. This design ensures the model can flexibly convert between different numerical representations and perform the corresponding mathematical operations. During task construction, we ensure that the numerical tokens involved in the tasks completely cover the entire numerical vocabulary  $V_{FP}$ . Through the two-phase fine-tuning tasks, the model acquires the ability to understand, manipulate, and generate sequences of numerical tokens, providing an efficient numerical encoding method for the subsequent traffic forecasting task.

### C. Multimodal Input Construction

Our method embeds the historical traffic information  $\mathbf{D}_{t-S+1:t}$  into the LLM context through the image encoder of a Vision-LLM, providing the model with a spatially-unabridged historical window that captures traffic data across

the entire geographical grid over a recent, finite time period. This approach enables the model to execute prediction tasks with a comprehensive understanding of the full spatial context of recent traffic dynamics, thereby improving its perceptual range and prediction accuracy. We convert the historical sequence of traffic matrices into an image format and input it into the image encoder to obtain image patch representations, which are then integrated into the LLM context for processing.

Since traffic data exhibits long-tail distribution characteristics while image encoders typically require input data within the  $[0, 1]$  range, we first perform normalization on the traffic data matrix  $D_t$ . For this purpose, we adopt Power-Law Normalization to obtain the normalized traffic matrix  $D_t^{(norm)}$ . This approach first applies a power transformation with an exponent  $p$  to each grid value to suppress the long tail and reduce the skewness of the data distribution [33]. Then, the result is divided by  $t_{max}^p$  to strictly map the values into the  $[0, 1]$  range. Here,  $p \in (0, 1]$  is a hyperparameter that controls the tail compression strength. The formula is as follows:

$$D_t^{(norm)} = \left[ \frac{(D_t^{(i,j)})^p}{t_{max}^p} \right]_{i,j}, \quad (8)$$

This normalization operation is performed on each input traffic data matrix to obtain the normalized global historical traffic information  $\{D_{t-S+1}^{(norm)}, \dots, D_t^{(norm)}\}$ .

A key consideration when inputting normalized traffic information into the image encoder of a Vision-LLM is the model's three-channel Red, Green, and Blue (RGB) structure. Visual encoders are pre-trained on natural images, where the R, G, and B channels are highly correlated and have learned tight statistical couplings, along with low-level features like edges and textures [34]. Directly mapping unrelated traffic variables to these three channels would introduce artificial cross-channel correlations and create a distributional mismatch with the pre-training data. This mismatch would prevent the model from effectively leveraging its pre-trained feature extraction capabilities. The challenge of this distributional mismatch is addressed by creating a pseudo-three-channel input, which involves replicating the single normalized traffic matrix across all three channels. This strategy ensures that the statistical properties of the input data remain consistent with the model's pre-training data. Consequently, the model can effectively activate its learned low-level feature extractors without being hindered by spurious color-based noise from uncorrelated channel information. This technique is a well-established practice in domains like medical imaging, where single-channel data such as X-rays are replicated to fit models pre-trained on RGB datasets like ImageNet [35]. We thus construct a grayscale image format:

$$I_t = [D_t^{(norm)}, D_t^{(norm)}, D_t^{(norm)}], \quad (9)$$

where  $I_t \in \mathbb{R}^{H \times W \times 3}$  represents the three-channel image corresponding to time step  $t$ , with  $H$  and  $W$  being the spatial dimensions of the traffic matrix. For any pixel at position  $(i, j)$  in the image, the RGB channel values are identical to normalized traffic values:

$$I_t[i, j, c] = D_t^{(norm)}[i, j], \quad c \in \{R, G, B\}, \quad (10)$$

where the index  $c$  iterates over the Red, Green, and Blue color channels. Through this approach, all normalized traffic matrices within the historical time window are converted into an image sequence  $\{I_{t-S+1}, I_{t-S+2}, \dots, I_t\}$ .

Next, we segment the image sequence into patches and process them through the Vision-LLM's image encoder. Setting the patch size of the image encoder to  $L \times L$ , each image  $I_t \in \mathbb{R}^{H \times W \times 3}$  can be segmented into  $N$  patches, where:

$$N = \lceil H/L \rceil \times \lceil W/L \rceil, \quad (11)$$

For each image  $I_k$  (where  $k \in \{t-S+1, \dots, t\}$ ) in the image sequence  $\{I_{t-S+1}, I_{t-S+2}, \dots, I_t\}$ , we segment it into a patch sequence:

$$\{\mathbf{p}_k^{(1)}, \mathbf{p}_k^{(2)}, \dots, \mathbf{p}_k^{(N)}\}, \quad (12)$$

where each patch  $\mathbf{p}_k^{(n)} \in \mathbb{R}^{L \times L \times 3}$ .

These patch sequences are then processed by the Vision-LLM's visual encoder. This operation, which we denote as  $\text{ImageEncoder}(\cdot)$ , transforms the patch sequence of a single image  $I_k$  into a corresponding sequence of visual embeddings  $E_k$ :

$$E_k = \text{ImageEncoder}(\{\mathbf{p}_k^{(1)}, \mathbf{p}_k^{(2)}, \dots, \mathbf{p}_k^{(N)}\}), \quad (13)$$

To construct the complete visual context for the entire historical window, these embedding sequences are concatenated in temporal order. This results in  $\mathbf{E}_{\text{visual}}$ , a single flattened sequence of embeddings that represents the global spatiotemporal traffic history:

$$\mathbf{E}_{\text{visual}} = [E_{t-S+1}, E_{t-S+2}, \dots, E_t], \quad (14)$$

Finally, these visual embeddings are concatenated with the text prompt embeddings to form the complete input context for the LLM:

$$\text{Context} = [\mathbf{E}_{\text{visual}}, \mathbf{E}_{\text{text}}], \quad (15)$$

where  $\mathbf{E}_{\text{text}}$  represents the embeddings of the text instructions, and  $\mathbf{E}_{\text{visual}} \in \mathbb{R}^{(S \times N) \times d}$  contains the complete 2D spatiotemporal traffic information from the historical window, with  $d$  being the embedding dimension.

#### D. SFT and Reinforcement Learning Optimization

After numerical alignment fine-tuning and multimodal input construction, the model has acquired the capability to process numerical tokens and understand global 2D spatiotemporal traffic information. To maximize predictive accuracy and ensure the generation of structurally correct outputs in traffic prediction tasks, our method employs a two-stage training strategy. The first stage uses SFT to establish a foundational predictive capability. In this phase, the model learns to imitate the ground-truth data, aligning its generative process with the task of mapping global historical traffic and cell-specific prompts to a corresponding future traffic sequence. The second stage then employs the GRPO method [16] to optimize this learned prediction strategy, further improving prediction accuracy.

1) *SFT Fine-tuning Stage*: In the SFT stage, we align the model’s generative process with the prediction task by training it on input-output pairs. For each training sample, we construct a single sequence by concatenating the complete input context with the corresponding ground-truth output sequence. The input context includes the image patches representing global historical traffic, the target cell’s geographical coordinates  $(x, y)$  as previously defined, its historical traffic data, and other metadata.

The model is then trained using a causal language modeling objective with *teacher-forcing* [36]. This involves maximizing the likelihood of the ground-truth tokens in the output sequence, conditioned on the preceding ground-truth tokens and the input context. Let  $\mathcal{T}$  be the set of indices corresponding to the tokens of the target output sequence. The loss is calculated using the cross-entropy objective, but only over the tokens in  $\mathcal{T}$ . This technique, often used in instruction-tuning [37], is formalized as

$$\mathcal{L}_{\text{SFT}} = -\frac{\sum_{i=1}^N \mathbb{I}[i \in \mathcal{T}] \log P_{\theta}(y_i | y_{<i}, x)}{\sum_{i=1}^N \mathbb{I}[i \in \mathcal{T}]}, \quad (16)$$

where  $N$  is the total sequence length,  $x$  is the input context,  $y_i$  is the token at position  $i$ , and  $\theta$  represents the model parameters. The term  $P_{\theta}$  denotes the conditional probability distribution over the vocabulary predicted by the model. The indicator function  $\mathbb{I}[i \in \mathcal{T}]$  implements loss masking. It equals 1 if the token at position  $i$  is part of the desired output, and 0 otherwise. This ensures that the loss is computed exclusively on the model’s predictions for the target sequence, ignoring the input context portion.

2) *GRPO Fine-tuning Stage*: Upon completing the SFT stage, the model has acquired basic traffic prediction capabilities, but its prediction strategy may not yet be optimal. To further enhance prediction accuracy, we employ a reinforcement learning optimization stage. Unlike traditional supervised learning that relies solely on historical labels, reinforcement learning allows for the direct optimization of prediction metrics. We specifically choose GRPO [16], a memory-efficient variant of Proximal Policy Optimization (PPO) [17]. Standard PPO is an actor-critic method that requires training a separate, computationally expensive critic network to estimate the value of states, which serves as a baseline for calculating advantages. GRPO innovatively foregoes this critic network, making it a more practical choice for fine-tuning large models.

The core mechanism of GRPO is to estimate the baseline advantage by leveraging group-wise comparisons. The optimization process unfolds as follows. First, for a given input prompt comprising the visual context and textual instructions, our ST-Vision-LLM acts as the policy network and generates not one, but a group of  $G$  candidate output sequences. Second, each of these  $G$  generated sequences is evaluated using a predefined reward function, yielding  $G$  scalar reward values. Third, instead of relying on a critic network, GRPO calculates a baseline directly from the group’s performance, typically the average reward of all  $G$  sequences. The relative advantage for any single sequence is then its reward compared to the group average. This process allows the model to discern better-than-

average predictions from worse-than-average ones within the sampled group.

Finally, the policy network is updated to increase the likelihood of generating sequences that achieve higher-than-average rewards. The GRPO objective function optimizes the policy by maximizing this group-relative advantage. To maintain training stability and prevent the policy from deviating too drastically from the well-behaved SFT model, the update is regularized by a KL-divergence penalty against a frozen reference model. The reference model is typically the initial SFT-tuned model. This entire process guides the model to learn a superior prediction strategy by directly optimizing for higher reward scores.

In our traffic prediction task, we define the reward function  $R$  as:

$$R = \exp\left(-\frac{\log 2}{x_h} \cdot \mathcal{E}\right) - \frac{|L_{\text{out}} - L_{\text{gt}}|}{L_{\text{gt}}} \cdot 0.5 + \delta_{\text{dec}}, \quad (17)$$

where  $\delta_{\text{dec}}$  is a penalty term for decoding failures, given by:

$$\delta_{\text{dec}} = \begin{cases} 0, & \text{successful decoding} \\ -0.5, & \text{decoding failure} \end{cases} \quad (18)$$

The term  $\mathcal{E}$  represents the Normalized Root Mean Square Error (NRMSE), which we define as:

$$\mathcal{E} = \frac{1}{d} \sqrt{\frac{1}{N} \sum_{k=1}^N (\hat{d}_k - d_k)^2}. \quad (19)$$

In these formulas,  $x_h$  is the half-score rate, a hyperparameter ensuring the reward is 0.5 when the error  $\mathcal{E}$  equals  $x_h$ . The term  $\exp(-\frac{\log 2}{x_h} \cdot \mathcal{E})$  is the accuracy reward component, valued in  $[0, 1]$ .  $L_{\text{gt}}$  is the length of the ground-truth sequence, and  $L_{\text{out}}$  is the length of the model’s output sequence. The term  $-\frac{|L_{\text{out}} - L_{\text{gt}}|}{L_{\text{gt}}} \cdot 0.5$  is a length mismatch penalty. In the NRMSE formula,  $N$  is the number of prediction steps,  $\hat{d}_k$  and  $d_k$  are the predicted and ground-truth values at step  $k$ , respectively, and  $d$  is a normalization constant. Training is terminated when the NRMSE on the validation set ceases to decrease, which yields the final trained model.

## V. EXPERIMENTS

In this section, we conduct a series of experiments to comprehensively evaluate the effectiveness of ST-Vision-LLM on spatio-temporal sequence forecasting tasks. Specifically, we first validate its benchmark performance on long-term and short-term prediction, as well as cross-domain prediction tasks. Subsequently, we further investigate the model’s performance in data-scarce and knowledge-transfer scenarios, such as few-shot learning, cross-domain few-shot fine-tuning, and zero-shot prediction, to fully demonstrate the few-shot learning and generalization capabilities of ST-Vision-LLM.

### Mobile Traffic Dataset

This study utilizes a public, real-world mobile traffic dataset originally released for the Telecom Italia Big Data Challenge [38]. The dataset contains measurements of total cellular traffic activity in the city of Milan and the Trentino province from November 1, 2013, to January 1, 2014 (a total of two months),

at a 10-minute observation interval. These two geographical areas differ significantly in nature and population density, thus exhibiting distinct traffic patterns. Specifically, the Milan area is divided into a  $100 \times 100$  grid of cells, where each cell covers an area of approximately 55,000 square meters (i.e.,  $235\text{m} \times 235\text{m}$ ). In contrast, the Trentino area consists of a  $117 \times 98$  grid of cells, with each cell covering an area of 1,000,000 square meters.

### Baseline Models

We compare ST-Vision-LLM against the following 12 baseline models, which can be categorized into four groups: (1) statistical models: ARIMA [18]; (2) models based on recurrent or convolutional neural networks: STN [6], ST-ResNet [20], ResLSTM [19], ACFM [24]; (3) models based on graph neural networks: STGCN [21], MSTGCN [23], GWNEN [22]; (4) models based on LLMs: ST-LLM [12], GCNGPT [12], GATGPT [25], Time-LLM [10]. The details of these baseline models are as follows:

- ST-LLM [12] defines the time steps at each location as tokens and designs a spatio-temporal embedding to learn the spatial positions and global temporal patterns of these tokens.
- GCNGPT [12] combines a graph convolutional network with a frozen pre-trained Transformer.
- GATGPT [25] fuses a graph attention mechanism with an LLM to enhance the understanding of spatial relationships.
- Time-LLM [10] reprograms the input time series via textual prototypes to align it with a frozen LLM.
- ACFM [24] employs an attention mechanism and consists of two progressive ConvLSTM units.
- GWNEN [22] introduces an adaptive adjacency matrix and combines it with stacked dilated 1D convolutions.
- ResLSTM [19] combines a residual network, a graph convolutional network, and a long short-term memory network.
- ST-ResNet [20] leverages a residual neural network framework to model temporal closeness, period, and trend.
- STGCN [21] integrates graph convolutional layers with convolutional sequence learning layers to handle spatio-temporal data.
- MSTGCN [23] adopts a multi-component approach to separately capture spatio-temporal correlations within different time periods.
- STN [6] fuses ConvLSTM and 3D-ConvNet architectures to extract spatio-temporal features.
- ARIMA [18] is an autoregressive integrated moving average model with a Kalman filter.

### Data Preprocessing and Experimental Setup

Due to data storage errors or improper transmission, some cellular cells have missing data for certain time periods, resulting in discontinuous traffic data. Therefore, data imputation is necessary before performing traffic forecasting. We employ **linear interpolation** to fill these gaps, a common

and robust practice for imputing short-term missing values in cellular traffic data that preserves temporal continuity without introducing strong distributional assumptions [39]. For any grid cell  $(x, y)$ , if its time series contains a sequence of consecutive missing values, we use linear interpolation for imputation. For example, for a sequence of missing values from time  $t_{start}$  to  $t_{end}$ , where  $d_{t_{start}}^{(x,y)}$  and  $d_{t_{end}}^{(x,y)}$  are known non-missing traffic values, the traffic value  $\tilde{d}_t^{(x,y)}$  at any time  $t$  between  $t_{start}$  and  $t_{end}$  (i.e.,  $t_{start} < t < t_{end}$ ) is calculated as:

$$\tilde{d}_t^{(x,y)} = d_{t_{start}}^{(x,y)} + \frac{t - t_{start}}{t_{end} - t_{start}} \left( d_{t_{end}}^{(x,y)} - d_{t_{start}}^{(x,y)} \right), \quad (20)$$

After data imputation, the model is trained using the complete imputed traffic data, which serves as both model input and training labels. However, during the model validation phase, treating imputed data as ground truth would introduce bias, compromising a fair evaluation. Therefore, although the model input still contains the imputed traffic data, the error computation for the output is performed only on the original observed data points, excluding the interpolated parts.

We train all deep learning models on data from November 1, 2013, to December 18, 2013 (48 days), validate them on the next 7 days of data, and then evaluate their performance on data from December 26, 2013, to January 1, 2014. We use Mean Absolute Error (MAE), Root Mean Squared Error (RMSE), and NRMSE to quantify the accuracy of our proposed ST-Vision-LLM and existing methods. They are defined as:

$$E_{\text{mae}} = \frac{1}{n} \sum_{i=1}^n |y_i - \hat{y}_i|, \quad (21)$$

$$E_{\text{rmse}} = \sqrt{\frac{1}{n} \sum_{i=1}^n (y_i - \hat{y}_i)^2}, \quad (22)$$

$$E_{\text{normse}} = \frac{E_{\text{rmse}}}{\bar{y}} = \frac{\sqrt{\frac{1}{n} \sum_{i=1}^n (y_i - \hat{y}_i)^2}}{\frac{1}{n} \sum_{i=1}^n y_i}, \quad (23)$$

Where  $\hat{y}_i$  is the predicted value,  $y_i$  is its corresponding ground truth value, and  $n$  is the total number of observed values in the sample. The metric  $E_{\text{normse}}$  is commonly used to evaluate model performance across datasets with different scales or units, as it normalizes the RMSE by the mean of the ground truth values, thereby eliminating the effect of scale. A lower metric value indicates a more accurate prediction.

Given computational cost constraints, in all datasets, we conduct training and validation only on the central region  $(x, y) \in [45, 55] \times [45, 55]$ . This means the model is tasked with predicting the output for this central sub-region only, although it can still perceive information from the entire input region. The experiments were conducted on an NVIDIA 5090 GPU with 32GB of memory.

To comprehensively compare the performance of ST-Vision-LLM with existing methods, we use five channels from the original dataset: Internet, sms\_in, sms\_out, call\_in, and call\_out. We select sms\_in for the SMS category and call\_in for the Call category. This yields six distinct telecommunication spatio-temporal traffic subsets, named Milan-Internet,

TABLE I

RESULTS OF LONG-TERM AND SHORT-TERM BASELINE PREDICTION. TRAINED AND EVALUATED ON MILAN-INTERNET, WITH THE INPUT SEQUENCE LENGTH SET TO  $S = 12$  AND PREDICTION HORIZONS SET TO  $K \in \{1, 10, 30, 60\}$ . THE BEST RESULT IS MARKED IN **BOLD** AND THE SECOND BEST IS UNDERLINED.

Horizon Metric	1-step			10-step			30-step			60-step		
	MAE	RMSE	NRMSE	MAE	RMSE	NRMSE	MAE	RMSE	NRMSE	MAE	RMSE	NRMSE
ST-Vision-LLM	<u>21.6525</u>	31.8887	0.1018	<b>27.4897</b>	<b>41.8479</b>	<b>0.1336</b>	<b>47.3410</b>	<b>70.9002</b>	<b>0.2258</b>	<b>75.8858</b>	<b>103.8315</b>	<b>0.3297</b>
ST-LLM	30.2360	41.5694	0.1325	51.5147	72.4567	0.2307	90.0111	149.3411	0.4747	109.3175	191.8308	0.6092
GCNGPT	29.5151	40.3999	0.1287	43.3770	58.4880	0.1862	77.5356	120.7583	0.3838	109.4818	195.0954	0.6195
GATGPT	30.3270	41.5221	0.1323	46.5658	65.2929	0.2079	89.1961	144.1842	0.4583	122.4923	208.4570	0.6619
Time-LLM	33.0400	45.3200	0.1447	56.7800	78.6500	0.2504	94.3400	151.9100	0.4828	132.4700	231.1900	0.7341
ACFM	28.1887	36.8261	0.1176	48.1180	76.4256	0.2433	79.0057	146.0898	0.4643	109.5715	183.7074	0.5833
GWNET	<b>14.9597</b>	<b>23.2448</b>	<b>0.0746</b>	<u>27.8492</u>	<u>42.5134</u>	<u>0.1353</u>	76.2321	140.6652	0.4471	103.8087	180.1602	0.5721
ResLSTM	34.8413	49.5176	0.1581	41.7371	59.8353	0.1905	<u>63.9126</u>	<u>85.6559</u>	<u>0.2723</u>	110.8396	147.7705	0.4696
STResNet	34.2675	46.4401	0.1480	49.3016	67.6645	0.2154	97.5731	165.3917	0.5257	139.4607	196.9013	0.6253
STGCN	21.6623	<u>28.5073</u>	<u>0.9100</u>	68.8386	91.8513	0.2924	83.3191	113.1243	0.3596	112.0226	153.3440	0.4870
MSTGCN	56.4753	87.0866	0.2782	93.1341	137.9330	0.4391	87.9280	129.3152	0.4110	<u>98.7467</u>	<u>144.8693</u>	<u>0.4601</u>
STN	39.5036	63.8600	0.2034	55.0212	91.1873	0.2903	80.7531	144.1812	0.4583	99.6591	177.8506	0.5648
ARIMA	40.2710	66.8839	0.2134	68.3513	113.3009	0.3607	125.4663	244.0582	0.7122	156.6109	291.2429	0.9249

TABLE II

EXPERIMENTAL RESULTS FOR CROSS-DOMAIN PREDICTION BASELINES. THE INPUT SEQUENCE LENGTH IS SET TO  $S = 12$ , AND THE PREDICTION HORIZON IS SET TO  $K = 36$ . THE BEST RESULT IS MARKED IN **BOLD** AND THE SECOND BEST IS UNDERLINED.

Dataset Metric	Trentino-Internet			Trentino-SMS			Milan-Internet			Milan-SMS		
	MAE	RMSE	NRMSE	MAE	RMSE	NRMSE	MAE	RMSE	NRMSE	MAE	RMSE	NRMSE
ST-Vision-LLM	<u>14.5816</u>	<b>30.4686</b>	<b>0.4393</b>	2.9704	<u>6.8868</u>	<u>0.8672</u>	<b>47.1007</b>	<b>66.9314</b>	<b>0.2126</b>	<b>7.2017</b>	<b>17.6204</b>	<b>0.7213</b>
ST-LLM	15.8334	35.1622	0.5069	2.8258	6.9871	0.8804	91.0541	154.3968	0.4904	8.9303	18.9329	0.7750
GCNGPT	17.0779	39.0128	0.5625	3.0729	7.4832	0.9428	83.8998	146.0534	0.4639	9.5920	18.8464	0.7715
GATGPT	<b>14.5254</b>	31.7930	0.4583	<b>2.7562</b>	<b>6.6744</b>	<b>0.8410</b>	103.7383	167.0780	0.5307	<u>8.9146</u>	<u>18.5483</u>	<u>0.7593</u>
Time-LLM	30.2154	66.4529	0.9582	5.5212	11.2638	1.4193	93.3401	175.6411	0.5579	16.8151	29.2006	1.1953
ACFM	16.6406	39.3074	0.5668	6.6483	13.4389	1.6934	113.4153	184.9829	0.5876	24.3491	37.5989	1.5391
MSTGCN	14.9153	<u>31.2775</u>	<u>0.4510</u>	6.2741	11.7457	1.4803	<u>72.8613</u>	<u>115.3424</u>	<u>0.3664</u>	15.4320	26.2068	1.0728
STN	15.0197	32.1622	0.4638	3.9015	8.7322	1.1003	83.7100	145.7200	0.4629	16.2560	27.3900	1.1212
ARIMA	45.2614	99.5753	1.4358	5.0521	10.5107	1.3244	125.4663	228.6892	0.7264	15.7524	26.3374	1.0781

Milan-SMS, Milan-Call, Trentino-Internet, Trentino-SMS, and Trentino-Call [38]. All subsequent tests are performed on these six subsets. In the benchmark and few-shot tests, we train and test the models on the SMS and Internet subsets. In the transfer learning and zero-shot tests, we first train the models on the Call subset and then perform transfer training and validation on the Internet and SMS subsets.

For methods using LLMs, Time-LLM [10] uses Qwen2.5-7B [40] as its backbone model, while our ST-Vision-LLM method uses Qwen2.5-VL-7B [41] as the base model for fine-tuning. As for the other comparative methods, we used the default configurations reported in their respective papers.

#### A. Long-term and Short-term Prediction Benchmark

*Setup:* We conduct evaluations on the Milan-Internet dataset, using the entire training set for training. The input sequence length  $S$  is set to 12 frames, with each frame spaced 10 minutes apart, corresponding to a 2-hour input window. We evaluate the model’s performance under different prediction horizons  $K$ , where  $K \in \{1, 10, 30, 60\}$  steps. These prediction steps correspond to 10 minutes, 1 hour, 40 minutes, 5 hours, and 10 hours, respectively. The evaluation metrics are MAE, RMSE, and NRMSE.

*Results:* Table I presents a performance comparison of ST-Vision-LLM against 12 baseline models across different prediction horizons. We can draw the following observations. (1) ST-Vision-LLM consistently outperforms all baseline models in multi-step and long-term prediction tasks. (2) Compared

to other LLM-based baselines, ST-Vision-LLM exhibits a significant advantage. For instance, in a 60-step prediction, ST-Vision-LLM reduces the NRMSE by approximately 45% compared to ST-LLM, demonstrating its superior capability in leveraging vision-language models for spatio-temporal forecasting. (3) When compared with state-of-the-art GNN-based models, we observe that GWNET demonstrates the strongest performance in single-step prediction. However, as the prediction horizon increases, the advantage of ST-Vision-LLM becomes apparent. In the 10-step prediction, ST-Vision-LLM’s performance is already slightly superior to GWNET, and its performance advantage further widens over longer prediction horizons, namely 30 and 60 steps. (4) Compared to traditional models based on recurrent or convolutional neural networks and statistical models, ST-Vision-LLM shows an overwhelming advantage across all prediction horizons. (5) A noteworthy observation is that the performance of many advanced baseline models degrades significantly as the prediction horizon increases, whereas ST-Vision-LLM’s error grows more gracefully, indicating its stronger robustness in capturing and extrapolating long-term spatio-temporal dependencies. Overall, the experimental results indicate that while ST-Vision-LLM shows competitive performance in single-step prediction, its true strength lies in multi-step and long-term forecasting, making it a powerful solution for spatio-temporal tasks that require reliable long-range predictions.

## B. Cross-domain Prediction Benchmark

*Setup:* To test the model’s long-term prediction accuracy across different domains, we conduct evaluations on four subsets: Trentino-Internet, Trentino-SMS, Milan-Internet, and Milan-SMS. The output sequence length  $K$  is set to 36 steps, corresponding to a 6-hour prediction window. Other experimental settings are consistent with the benchmark test in Section A.

*Results:* Table II shows the cross-domain prediction results on four different subsets. We can draw the following observations. (1) ST-Vision-LLM achieves the best performance on three of the subsets and consistently demonstrates superior prediction accuracy across all four. (2) Compared to other LLM-based baselines, ST-Vision-LLM shows consistent superiority. Interestingly, GATGPT exhibits strong competitiveness on the Trentino datasets, but its performance declines on the Milan datasets, suggesting that ST-Vision-LLM has stronger generalization capability across different data domains. (3) When compared with advanced GNN-based models, ST-Vision-LLM also shows a significant advantage. For example, on the Milan-Internet dataset, ST-Vision-LLM reduces the RMSE by over 42% compared to the second-best model, MSTGCN. (4) Traditional statistical models and models based on recurrent or convolutional neural networks, such as ARIMA and STN, lag significantly in performance across all test scenarios, highlighting the advantages of modern approaches in handling complex spatio-temporal data. In summary, these cross-domain prediction results provide strong evidence of ST-Vision-LLM’s robustness and adaptability across different geographical regions and data types, underscoring its potential as a general-purpose spatio-temporal forecasting framework.

## C. Few-shot Prediction

TABLE III

EXPERIMENTAL RESULTS FOR 10% FEW-SHOT PREDICTION IN TERMS OF NRMSE. THE INPUT SEQUENCE LENGTH IS SET TO  $S = 12$ , AND THE PREDICTION HORIZON IS SET TO  $K = 36$ . TRAINED USING 10% OF THE DATASET. THE BEST RESULT IS MARKED IN **BOLD** AND THE SECOND BEST IS UNDERLINED.

Method	Trentino-Internet	Trentino-SMS	Milan-Internet	Milan-SMS
ST-Vision-LLM	<u>0.6357</u>	<b>0.9882</b>	<b>0.2537</b>	<b>0.7324</b>
ST-LLM	0.6979	1.3362	0.4555	0.8901
GCNGPT	0.7363	1.4068	<u>0.4410</u>	<u>0.8575</u>
GATGPT	<b>0.5249</b>	<u>1.1700</u>	0.5154	0.8679
Time-LLM	0.9616	1.3615	0.5639	0.9315
STN	1.1736	1.3032	0.6696	0.9223

*Setup:* LLMs, benefiting from their extensive pre-training data, often exhibit excellent few-shot learning capabilities [42]. This ability is particularly advantageous in data-scarce scenarios. In this section, we follow the configuration of the benchmark test in Section C. Building on this, we evaluate the few-shot learning capability of each method by limiting the amount of training data (i.e., using only the first 10% and 5% of the training data).

TABLE IV

EXPERIMENTAL RESULTS FOR 5% FEW-SHOT PREDICTION IN TERMS OF NRMSE. THE INPUT SEQUENCE LENGTH IS SET TO  $S = 12$ , AND THE PREDICTION HORIZON IS SET TO  $K = 36$ . TRAINED USING 5% OF THE DATASET. THE BEST RESULT IS MARKED IN **BOLD** AND THE SECOND BEST IS UNDERLINED.

Method	Trentino-Internet	Trentino-SMS	Milan-Internet	Milan-SMS
ST-Vision-LLM	<u>0.7451</u>	<b>1.0505</b>	<b>0.3887</b>	<b>0.6801</b>
ST-LLM	0.7678	1.5191	0.5100	<u>0.8892</u>
GCNGPT	0.8004	1.4890	<u>0.4379</u>	0.9936
GATGPT	<b>0.6354</b>	<u>1.4071</u>	0.5209	0.9302
Time-LLM	0.9668	1.4622	0.5403	1.2338
STN	1.6943	1.4863	1.4616	1.1412

*Results:* Tables III and IV present the results of the few-shot learning tests using 10% and 5% of the data, respectively. We can draw the following observations. ST-Vision-LLM achieves the best performance in most test scenarios; specifically, it is optimal on three out of the four subsets with both 10% and 5% of the training data. Compared to other LLM-based baselines, ST-Vision-LLM demonstrates a significant superiority. A notable exception is GATGPT, which consistently performs best on the Trentino-Internet dataset, suggesting that GATGPT may have unique advantages in handling specific data types. In contrast, the traditional STN model performs the worst in all few-shot tests, highlighting the advantage of modern architectures in terms of data efficiency. Taken together, these results provide strong evidence of ST-Vision-LLM’s superior few-shot learning capabilities, making it highly suitable for data-constrained spatio-temporal prediction applications.

## D. Cross-Domain Few-Shot Fine-Tuning Prediction

TABLE V

EXPERIMENTAL RESULTS FOR CROSS-DOMAIN FEW-SHOT FINE-TUNING FROM THE **TRENTINO-CALL** SOURCE DOMAIN IN TERMS OF NRMSE. THE INPUT SEQUENCE LENGTH IS SET TO  $S = 12$ , AND THE PREDICTION HORIZON IS SET TO  $K = 36$ . MODELS ARE FINE-TUNED USING 2% OF THE TARGET DOMAIN’S TRAINING DATA. THE BEST RESULT IS MARKED IN **BOLD** AND THE SECOND BEST IS UNDERLINED.

Method	Trentino-Internet	Trentino-SMS	Milan-Internet	Milan-SMS
ST-Vision-LLM	<b>0.6638</b>	<b>0.9548</b>	<b>0.2150</b>	<b>0.7126</b>
ST-LLM	1.0469	1.6283	0.5074	0.9318
GCNGPT	0.9999	1.6218	<u>0.4819</u>	<u>0.9828</u>
GATGPT	<u>0.7790</u>	1.4709	0.5071	0.9918
Time-LLM	0.9939	1.4384	0.5456	1.2201
STN	1.0076	<u>1.3208</u>	0.7980	0.9913

*Setup:* In addition to few-shot learning, LLMs are also widely recognized for their strong cross-domain learning and knowledge transfer capabilities [43]. This means that a model fully trained on one domain can achieve excellent performance on another domain with only a small amount of fine-tuning. We refer to this phenomenon as cross-domain transfer capability. For instance, we study a model’s performance on one dataset after being trained on another. In this subsection, to evaluate the cross-domain transfer capability of each method, we follow the benchmark setup from Section C with

the following modification: first, the models are pre-trained on the complete Trentino-Call dataset. Subsequently, these pre-trained models are fine-tuned on the Trentino-Internet, Trentino-SMS, Milan-Internet, and Milan-SMS datasets, respectively, using only 2% of their training data, and then their performance is evaluated.

*Results:* Table V shows the performance comparison of the methods in the cross-domain few-shot fine-tuning scenario. The results clearly indicate that ST-Vision-LLM achieves the best performance on all four subsets, demonstrating its superior knowledge transfer and fine-tuning capabilities. A noteworthy phenomenon is that other LLM-based baselines exhibit inconsistent performance. For example, GATGPT performs second-best on the Trentino-Internet dataset but not on others, while the traditional STN model unexpectedly achieves the second-best result on the Trentino-SMS dataset but performs poorly in other, more complex scenarios. In contrast, ST-Vision-LLM maintains its leading position across all tests. This is particularly evident on the Milan-Internet dataset, which further highlights ST-Vision-LLM’s exceptional ability to maintain consistent high performance across different data domains. In summary, these results demonstrate that ST-Vision-LLM can efficiently adapt to new domains and achieve state-of-the-art prediction accuracy even when fine-tuned with a very small amount of data from the target domain.

### E. Zero-Shot Prediction

TABLE VI

EXPERIMENTAL RESULTS FOR ZERO-SHOT PREDICTION FROM THE TRENTINO-CALL SOURCE DOMAIN IN TERMS OF NRMSE. THE INPUT SEQUENCE LENGTH IS SET TO  $S = 12$ , AND THE PREDICTION HORIZON IS SET TO  $K = 36$ . MODELS ARE EVALUATED DIRECTLY ON THE TARGET DOMAIN. THE BEST RESULT IS MARKED IN **BOLD** AND THE SECOND BEST IS UNDERLINED.

Method	Trentino-Internet	Trentino-SMS	Milan-Internet	Milan-SMS
ST-Vision-LLM	<b>1.0975</b>	<b>1.0541</b>	<b>0.4047</b>	<b>0.7560</b>
ST-LLM	1.4578	2.2119	0.4940	1.2128
GCNGPT	1.2596	1.6848	<u>0.4384</u>	<u>0.8171</u>
GATGPT	1.4012	1.7934	0.4565	0.8515
Time-LLM	<u>1.1317</u>	<u>1.5298</u>	0.6253	1.3527
STN	1.2480	1.6420	0.8626	1.1715

*Setup:* LLMs also have great potential as effective zero-shot learners [42]. In this setup, we evaluate the zero-shot learning capability of ST-Vision-LLM within a cross-domain transfer framework. We fully train a model on one dataset and directly evaluate its performance on another, during which the model is not exposed to any data samples from the target domain. We pre-train the models on Trentino-Call and then directly evaluate them on the Trentino-Internet, Trentino-SMS, Milan-Internet, and Milan-SMS datasets, with other experimental settings remaining consistent with those in Section D.

*Results:* Table VI shows the performance of each method on the zero-shot prediction task. The experimental results clearly demonstrate that ST-Vision-LLM achieves the best performance across all four target domains, providing strong evidence of its superior zero-shot generalization capabilities.

Notably, while the second-best performing model varies across datasets, ST-Vision-LLM consistently remains in the lead. For example, on the Milan-Internet dataset, ST-Vision-LLM reduces the NRMSE by approximately 7.7% compared to the second-best model, GCNGPT, and by over 18% compared to ST-LLM. In contrast, other baseline models, particularly traditional ones like STN and some LLM-based methods like ST-LLM, exhibit a significant performance degradation in the zero-shot scenario. These results indicate that ST-Vision-LLM can effectively transfer knowledge learned from a source domain to unseen target domains without any fine-tuning, thereby demonstrating its potential as a powerful zero-shot predictor.

## VI. CONCLUSION

ST-Vision-LLM reframes spatiotemporal traffic forecasting as a vision-language problem, encoding historical data as visual patches for global context and using textual prompts for targeted predictions. A core innovation is our numerical encoding scheme, combined with a two-stage alignment fine-tuning, which endows the LLM with essential numeracy. The framework achieves state-of-the-art performance, demonstrating exceptional generalization and data efficiency, especially in few-shot, cross-domain, and zero-shot scenarios. This validates our hypothesis that leveraging the global context of Vision-LLMs overcomes the limitations of traditional models, establishing a powerful and generalizable new paradigm for spatiotemporal prediction.

## REFERENCES

- [1] Q. Wen, T. Zhou, C. Zhang, W. Chen, Z. Ma, J. Yan, and L. Sun, “Transformers in Time Series: A Survey,” in *Proc. IJCAI*, 2023.
- [2] S. Hochreiter and J. Schmidhuber, “Long Short-Term Memory,” *Neural Computation*, vol. 9, no. 8, pp. 1735–1780, 1997.
- [3] S. Bai, J. Z. Kolter, and V. Koltun, “An Empirical Evaluation of Generic Convolutional and Recurrent Networks for Sequence Modeling,” *arXiv:1803.01271*, 2018.
- [4] Y. Li, R. Yu, C. Shahabi, and Y. Liu, “Diffusion Convolutional Recurrent Neural Network: Data-Driven Traffic Forecasting (DCRNN),” in *Proc. ICLR*, 2018.
- [5] B. Yu, H. Yin, and Z. Zhu, “Spatio-Temporal Graph Convolutional Networks: A Deep Learning Framework for Traffic Forecasting (STGCN),” in *Proc. IJCAI*, 2018.
- [6] C. Zhang and P. Patras, “Long-Term Mobile Traffic Forecasting Using Deep Spatio-Temporal Neural Networks,” in *Proc. ACM MobiHoc*, 2018.
- [7] Y. Nie, N. Ma, J. Shang, J. Yu, and L. Chen, “A Time Series is Worth 64 Words: Long-term Forecasting with Transformers (PatchTST),” in *Proc. ICLR*, 2023.
- [8] H. Wu, J. Xu, J. Wang, and M. Long, “Autoformer: Decomposition Transformers with Auto-Correlation for Long-Term Series Forecasting,” in *Proc. NeurIPS*, 2021.
- [9] Y. Chang, Y. Li, and Y. Zhang, “LLM4TS: Two-Stage Fine-Tuning for Time Series with Large Language Models,” *ACM TKDD*, 2024.
- [10] X. Jin, Y. Wang, Y. Li, and Y. Zhang, “Time-LLM: Time Series Forecasting by Reprogramming Large Language Models,” in *Proc. ICLR*, 2024.
- [11] T. Zhou, Z. Ma, Q. Wen, J. Wang, L. Sun, and R. Jin, “One Fits All: Power General Time Series Analysis by Pretrained LM (FPT),” in *Proc. NeurIPS*, 2023.
- [12] Y. Liu, Y. Wang, and Y. Zhang, “Spatial-Temporal Large Language Model for Traffic Prediction (ST-LLM),” 2024.
- [13] L. Liu, S. Yu, R. Wang, Z. Ma, and Y. Shen, “How Can Large Language Models Understand Spatial-Temporal Data? (STG-LLM),” *arXiv:2401.14192*, 2024.

- [14] H. Jeon, H. Lee, J. Kim, and S. Ko, "ST-LINK: Spatially-Aware Large Language Models for Spatio-Temporal Forecasting," in *Proc. ACM CIKM*, 2025.
- [15] Y. Li, Y. Wang, and Y. Zhang, "UrbanGPT: Spatio-Temporal Large Language Models," in *Proc. KDD*, 2024.
- [16] DeepSeek-AI (Y. Liu *et al.*), *DeepSeekMath: Pushing the Limits of Mathematical Reasoning in Open Language Models*, arXiv, 2024.
- [17] J. Schulman, F. Wolski, P. Dhariwal, A. Radford, and O. Klimov, "Proximal Policy Optimization Algorithms," *arXiv preprint arXiv:1707.06347*, 2017.
- [18] G. E. P. Box, G. M. Jenkins, G. C. Reinsel, and G. M. Ljung, *Time Series Analysis: Forecasting and Control*, 5th ed., Wiley, 2015.
- [19] J. Zhang, F. Chen, Z. Cui, Y. Guo, and Y. Zhu, "Deep Learning Architecture for Short-Term Passenger Flow Forecasting in Urban Rail Transit," *IEEE Trans. Intell. Transp. Syst.*, 2020.
- [20] J. Zhang, Y. Zheng, and D. Qi, "Deep Spatio-Temporal Residual Networks for Citywide Crowd Flows Prediction," in *Proc. AAAI*, 2017, pp. 1655–1661.
- [21] B. Yu, H. Yin, and Z. Zhu, "Spatio-Temporal Graph Convolutional Networks: A Deep Learning Framework for Traffic Forecasting," in *Proc. IJCAI*, 2018, pp. 3634–3640.
- [22] Z. Wu, S. Pan, G. Long, J. Jiang, and C. Zhang, "Graph WaveNet for Deep Spatial-Temporal Graph Modeling," in *Proc. IJCAI*, 2019, pp. 1907–1913.
- [23] S. Guo, Y. Lin, N. Feng, C. Song, and H. Wan, "Attention Based Spatial-Temporal Graph Convolutional Networks for Traffic Flow Forecasting," in *Proc. AAAI*, 2019, pp. 922–929.
- [24] L. Liu, R. Zhang, J. Peng, G. Li, B. Du, and L. Lin, "Attentive Crowd Flow Machines," in *Proc. ACM Multimedia*, 2018, pp. 1553–1561.
- [25] Y. Chen, X. Wang, and G. Xu, "GATGPT: A Pre-trained Large Language Model with Graph Attention Network for Spatiotemporal Imputation," *arXiv:2311.14332*, 2023.
- [26] M. Garnelo, J. Schwarz, D. Rosenbaum, F. Viola, D. J. Rezende, S. M. A. Eslami, Y. W. Teh, "Conditional Neural Processes," *Proceedings of the 35th International Conference on Machine Learning (ICML)*, 2018.
- [27] F. Charton, *Linear Algebra with Transformers*, Transactions on Machine Learning Research, 2022.
- [28] E. J. Hu, Y. Shen, P. Wallis, Z. Allen-Zhu, Y. Li, S. Wang, L. Wang, W. Chen, "LoRA: Low-Rank Adaptation of Large Language Models," in *Proc. ICLR*, 2022.
- [29] T. B. Brown, B. Mann, N. Ryder, M. Subbiah, J. D. Kaplan, P. Dhariwal, A. Neelakantan, P. Shyam, G. Sastry, A. Askell, S. Agarwal, A. Herbert-Voss, G. Krueger, T. Henighan, R. Child, A. Ramesh, D. M. Ziegler, J. Wu, C. Winter, C. Hesse, M. Chen, E. Sigler, M. Litwin, S. Gray, B. Chess, J. Clark, C. Berner, S. McCandlish, A. Radford, I. Sutskever, D. Amodei, "Language Models are Few-Shot Learners," *Advances in Neural Information Processing Systems 33 (NeurIPS)*, 2020.
- [30] M. Geva, A. Gupta, J. Berant, "Injecting Numerical Reasoning Skills into Language Models," *Proceedings of the 58th Annual Meeting of the Association for Computational Linguistics (ACL)*, 2020.
- [31] E. Akyürek, D. Schuurmans, J. Andreas, T. Ma, D. Zhou, "What Learning Algorithm Is In-Context Learning? Investigations with Linear Models," *International Conference on Learning Representations (ICLR)*, 2023.
- [32] N. Shazeer, "GLU Variants Improve Transformer," *arXiv:2002.05202*, 2020.
- [33] G. E. P. Box, D. R. Cox, "An Analysis of Transformations," *Journal of the Royal Statistical Society: Series B (Methodological)*, 1964, 26(2): 211–252.
- [34] Y. Xie, D. Richmond, "Pre-training on Grayscale ImageNet Improves Medical Image Classification," *Proceedings of the European Conference on Computer Vision Workshops (ECCVW)*, 2018.
- [35] P. R. A. S. Bassi, R. Attux, "Covid-19 detection using chest X-rays: is lung segmentation important for generalization?" *Research on Biomedical Engineering*, vol. 38, pp. 1121–1139, 2022.
- [36] C. Raffel, N. Shazeer, A. Roberts, *et al.*, "Exploring the Limits of Transfer Learning with a Unified Text-to-Text Transformer," *Journal of Machine Learning Research*, 2020.
- [37] L. Ouyang, J. Wu, X. Jiang, *et al.*, "Training language models to follow instructions with human feedback," *NeurIPS*, 2022.
- [38] G. Barlacchi, M. De Nadai, R. Larcher, A. Casella, C. Chitic, G. Torrisi, F. Antonelli, A. Vespignani, A. Pentland, and B. Lepri, *A multi-source dataset of urban life in the city of Milan and the Province of Trentino*, *Scientific Data*, vol. 2, Article 150055, 2015.
- [39] S. Zhao, X. Jiang, G. Jacobson, R. Jana, W.-L. Hsu, R. Rustamov, M. Talasila, S. A. Aftab, Y. Chen, and C. Borcea, "Cellular Network Traffic Prediction Incorporating Handover: A Graph Convolutional Approach," in *Proc. 17th IEEE Int'l Conf. on Sensing, Communication, and Networking (SECON)*, 2020.
- [40] A. Yang, B. Yang, B. Zhang, B. Hui, B. Zheng, B. Yu, C. Li, D. Liu, F. Huang, H. Wei, *et al.*, *Qwen2.5 Technical Report*, arXiv:2412.15115, 2024.
- [41] S. Bai, K. Chen, X. Liu, J. Wang, W. Ge, S. Song, K. Dang, P. Wang, S. Wang, J. Tang, *et al.*, *Qwen2.5-VL Technical Report*, arXiv:2502.13923, 2025.
- [42] T. B. Brown, B. Mann, N. Ryder, *et al.*, "Language Models are Few-Shot Learners," *NeurIPS*, 2020.
- [43] C. Raffel, N. Shazeer, A. Roberts, *et al.*, "Exploring the Limits of Transfer Learning with a Unified Text-to-Text Transformer," *Journal of Machine Learning Research*, 2020.